12th International Symposium on Turbulence and Shear Flow Phenomena (TSFP12)
Osaka, Japan, July 19–22, 2022

RESOLVENT ANALYSIS OF TURBULENT PIPE FLOW LADEN WITH LOW INERTIA PARTICLES

Rasmus Korslund Schlander
Department of Aeronautics
Imperial College London
London SW7 2AZ, United Kingdom
r.schlander19@imperial.ac.uk

George Papadakis
Department of Aeronautics
Imperial College London
London SW7 2AZ, United Kingdom
g.papadakis@imperial.ac.uk

Stelios Rigopoulos
Department of Mechanical Engineering
Imperial College London
London SW7 2AZ, United Kingdom
s.rigopoulos@imperial.ac.uk

ABSTRACT

We extend the resolvent framework to turbulent flows laden with low inertia particles. The particle velocities are modelled using the equilibrium Eulerian model, which is valid for Stokes numbers up to 1. We analyse a vertical turbulent pipe flow with a Reynolds number of 5300 based on diameter and bulk velocity, for Froude numbers $Fr = 0.4, -0.4$ and Stokes numbers $St^+ = 0 - 1$. A direct numerical simulation (DNS) for a pipe with a length of 7.5 diameters (D) is performed with the particles released uniformly at the pipe inlet. The resolvent formulation can predict some of the physical phenomena observed in inertial particle flows such as localized high concentration due to the vortical centrifuge effect, turbophoresis and gravitational effects. It is shown that the upward flow increases particle concentration in the log layer of the pipe. The downward flow increases concentration near the centre of the pipe: both features have been observed in previous Lagrangian simulations as well as experiments. The main effect of Stokes number is the amplification of smaller streamwise wavelengths, therefore, increasing local scale clustering of particles. The effect of the direction of gravity was also reproduced using a simplified resolvent model which did not require a mean concentration profile as input and simplifies the analysis since no prior simulation or experiment is required for the model to work.

INTRODUCTION

The interaction between inertial particles and coherent flow structures plays an important role in particle deposition in wall-bounded turbulent flows. Understanding this interaction can lead to better control over mixing and deposition in pipes and channels. One of the methods used for analysing coherent structures in flows is resolvent analysis. This is an equation-driven approach, where the non-linear terms are treated as random forcing to the linear system. The resolvent operator then maps these inputs (forcings) to the outputs (responses). Recently, this method has been extended to scalars (Dawson *et al.* (2018)) and geophysical flows using the Boussinesq approximation (Ahmed *et al.* (2021)). This paper presents another extension of the resolvent analysis framework to particle transport which is modelled using an Eulerian description that is valid for particles of low inertia. This allows us to analyse the interaction between coherent structures and inertial particles, and can potentially allow us to derive low rank descriptions of these complex interactions.

METHODOLOGY

We consider the turbulent flow inside a circular pipe with a particles injected at the inlet. The flow is assumed to be incompressible and the continuity, momentum and particle transport equations are written in Cartesian tensor notation as:

$$\frac{\partial u_i}{\partial x_i} = 0, \tag{1}$$

$$\frac{\partial u_i}{\partial t} + \frac{\partial u_i u_j}{\partial x_j} = -\frac{\partial p}{\partial x_i} + \frac{1}{Re}\frac{\partial^2 u_i}{\partial x_j \partial x_j}, \tag{2}$$

$$\frac{\partial c}{\partial t} + v_j \frac{\partial c}{\partial x_j} = \frac{1}{ReSc}\frac{\partial^2 c}{\partial x_j \partial x_j}, \tag{3}$$

where u_i, v_i are the instantaneous fluid and particle velocities in the i-th direction respectively, p is the pressure, t is the time, and c is the particle concentration. The notation (x_1, x_2, x_3) for the spatial coordinates is used interchangeably with the notation (x, y, z), where $z = x_3$ is the axial, i.e. streamwise, direction. Due to rotational symmetry, it is also convenient to use polar coordinates (r, θ, z), where $(x, y) = (r\cos\theta, r\sin\theta)$. All variables are non-dimensionalised with the reference quantities being the bulk velocity U_B, the pipe diameter D, and the inlet concentration c_I. The Reynolds number is defined as $Re = \frac{U_B D}{\nu}$, where ν is the kinematic viscosity, and the Schmidt

number as $Sc = \frac{\nu}{\alpha}$, where α is the particle diffusivity. The mean (i.e. time-average) and fluctuating quantities are denoted using an overbar and a prime, for example $\bar{c}$ and c', respectively.

The particle velocity, v_i, is estimated by assuming that the material derivative of the particle is approximately equal to the material derivative of the fluid and is known as the Eulerian method, Ferry & Balachandar (2001):

$$v_i = u_i - \tau\left(\frac{\mathrm{D}u_i}{\mathrm{D}t} - g_i\right) \tag{4}$$

where τ is the particle relaxation time,

$$\tau = \frac{\left(\rho_\mathrm{p} + \frac{1}{2}\rho_\mathrm{f}\right) D_p^2}{18\mu_\mathrm{f}} \tag{5}$$

and ρ_p is the particle density, ρ_f is the fluid density, D_p is the particle diameter, μ_f is the dynamic viscocity of the fluid and $\frac{D}{Dt}$ is the material derivative. By inserting this into equation 3 and non-dimensionalizing using $Fr_i = \frac{U_B^2}{g_i D}$ and $St = \frac{\tau U_B}{D}$, we obtain:

$$\frac{\partial c}{\partial t} + \left(u_j + St\left(\frac{1}{Fr_i} - \frac{\partial u_j}{\partial t} - u_k\frac{\partial u_j}{\partial x_k}\right)\right)\frac{\partial c}{\partial x_j} = \frac{1}{ReSc}\frac{\partial^2 c}{\partial x_j \partial x_j}, \tag{6}$$

This model for particle flow assumes that the particle concentration is small, which means there will be no collisions, and that all particles within a cell move in the same direction, i.e. no particle crossings.

We here note that 3 different Stokes numbers are used throughout this work; $St = \tau U_B/D$ based on bulk values, $St^+ = \tau u_\tau^2/\nu$ based on wall values, where u_τ is the friction velocity and $St_k = \tau/\tau_k = (2\rho_p + 1)/36\left(\frac{D_p}{\eta}\right)^2$ is based on the Kolmogorov time and length scale, τ_k and η, respectively. In the present simulation, St and St^+ are found to be maximum 0.04 and 1.0, respectively. St_k depends on the Kolmogorov length scale, which changes with the radial direction in the pipe and it is found to be maximum 1.12.

We validate the velocity field obtained using the equilibrium Eulerian method, to the Lagrangian simulations of a turbulent channel flow with $Re_\tau = 180$ from Ferry *et al.* (2003) and a pipe flow simulation with $Re_\tau = 323$ compared to the experiment of Oliveira *et al.* (2017) and the DNS of Veenman (2004). The channel flow is simulated using $N_c = 9.3\times10^6$ cells, with $(N_x, N_y, N_z) = (256, 128, 256)$ and dimensions, $(L_x, Ly, L_z) = (4\pi, 2, 4/3\pi)$. We can observe in figure 1a that for $St^+ = 1$ the mean radial particle velocity matches the Lagrangian simulation well, and reasonably well for $St^+ = 3$. However, for the difference in average streamwise fluid and particle velocity in figure 1b, we start to observe some differences near the peak for $St^+ = 1$ as well as a significant deviation in most of the pipe for $St^+ = 3$. This means that the model is deemed accurate for Stokes numbers up to $St^+ = 1$. The pipe flow simulation has $N_c = 2.6\times10^7$ cells on a grid that near the centre is H-type and transitions to O-type closer to the wall to fit the cylindrical boundary, with $\Delta r^+_{wall} = 0.1$, $\Delta\theta r^+_{max} = 4.84$, $\Delta r^+_{center,max} = 2.63$ and $\Delta z^+_{max} = 8.2$. The mean of the mean particle field, plotted in figure 1c, show an excellent agreement for $St^+ = 1.47$. Mean and RMS values of the fluid velocity field have also been validated for both simulations, but are omitted here for brevity.

A database of mean velocity and concentration profiles are needed for the Resolvent analysis and 20 different flow configurations were therefore simulated for $St^+ = 0.1, 0.2, 0.5, 1.0$ and $Fr = -4, -0.4, 0, 4, -4$ as well as the special case where gravity is omitted ($Fr \to \infty$) for a pipe flow with $Re_\tau = 180$. The mean and RMS plots are, once again, omitted here for brevity.

An in-depth introduction to the resolvent framework can be found among others in McKeon & Sharma (2010); McKeon (2017). In this paper, we extend the resolvent analysis further to understand the behaviour of low inertia particles in turbulent pipe flows. We analyse a fully developed turbulent pipe flow that transports low-inertia particles. The flow is assumed homogeneous in the streamwise direction and stationary in time, which means the instantaneous velocity $u = [u_z, u_r, u_\theta]$, pressure and particle concentration fields, defined together as $q = [u, p, c]$, can be expressed as a superposition of Fourier modes with streamwise wavenumber k_z, azimuthal wavenumber k_θ (constrained to be an integer), and frequency ω,

$$\mathbf{q}'(r,\theta,z,t) = \sum_{k_\theta}\int_{-\infty}^{\infty}\int_{-\infty}^{\infty}\begin{bmatrix}\hat{u}(r;k_z,k_\theta,\omega)\\ \hat{p}(r;k_z,k_\theta,\omega)\\ \hat{c}(r;k_z,k_\theta,\omega)\end{bmatrix} e^{\mathrm{i}(k_z z + k_\theta\theta - \omega t)}dk_z d\omega \tag{7}$$

where $\hat{()}$ denotes a Fourier transformed variable. This decomposition leads to each wavenumber-frequency combination $k = (k_z, k_\theta, c_w = \omega/k_z)$ and represents a helical wave moving downstream with wave speed, c_w, for $k = (k_z, k_\theta, \omega) \neq (0,0,0)$. Furthermore, wavelengths are defined as $\lambda_z = L_z\pi/k_z$ and $\lambda_\theta = D\pi/k_\theta$. Finally, the critical layer is defined as where the wave speed, c_w, is equal to the mean streamwise velocity, i.e., $c_w = \overline{u}(y_c)$. Using this Fourier representation, at each wavenumber-frequency combination, k, the convection diffusion equation can be expressed in dimensionless form as:

$$\begin{aligned}&(-i\omega + ik_z\overline{u}_z)c' + u'_r\tfrac{\partial\overline{c}}{\partial r} + \\ &St\left(i\omega u'_r\tfrac{\partial\overline{c}}{\partial r} - 2ik_z u'_r\tfrac{\partial\overline{u}_z}{\partial r}\overline{c} - ik_z u'_r\overline{u}_z\tfrac{\partial\overline{c}}{\partial r}\right) + \\ &\tfrac{St}{Fr}ik_z c' - Re^{-1}Sc^{-1}\nabla^2 c' - \Theta_s = f_c\end{aligned} \tag{8}$$

where a source term, Θ_s, is added to ensure streamwise homogeneity. Equation (8) and the corresponding equations for the flow are re-arranged to obtain a forcing–response relationship:

$$\tilde{q} = H_k f_k \tag{9}$$

where $f_k = [f_u, 0, f_c]$ is the velocity and scalar forcing and H_k is the resolvent operator. The resolvent operator is discretized in the radial direction using a Chebyshev pseudospectral method.

We chose the following energy norm, also previously previously been analysed in Dawson *et al.* (2018),

$$E = \frac{1}{2}\int_\Omega\left(\alpha u^2 + \beta c^2\right)dV \tag{10}$$

where α is the weight of the velocity field, β is the weight of the particles in the norm. For $\beta = 0$, we obtain the kinetic energy norm. Here it must be noted, that by setting $\alpha = 0$, we simplify the resolvent operator to the equation:

$$c'\left(ik_z\overline{u}_z - i\omega - \frac{\Delta}{ReSc} + ik_z\frac{St}{Fr} - \Theta_{s,c}\right) = f_c \tag{11}$$

which is independent of $\bar{c}$. By performing the SVD on the resolvent operator, H_s, we obtain the following decomposition

$$H_s(k) = \sum_{j=1}^{\infty} \sigma_j(k)\hat{\psi}_j(r;k)\hat{\phi}_j^*(r;k) \tag{12}$$

where ϕ is the forcing mode, ψ is the response mode and σ is the gain related to each response mode.

RESULTS

The resolvent gain, σ, provides information about how the system reacts to a forcing. The larger the gain, the more sensitive the system is to the corresponding forcing (or input). The system is said to be low rank if a significant part of the total gain is captured by the first mode. Individual weights for the modes are needed for describing the full forcing and response system, however, past studies such as McKeon & Sharma (2010), Sharma & McKeon (2013) have shown that broadband forcing can be used to describe important features in the flow, which can also be observed in experiments. We are therefore checking if the operator is low rank i.e.,

$$H_s(k) \approx \sigma_1 \hat{\psi}_1 \hat{\phi}_1^*. \tag{13}$$

Low-rank behaviour typically indicates that there is a dynamically significant spatio-temporal structure defined by k. We study how long rank behaviour changes with St^+ by plotting the gain of the first resolvent mode relative to the gain from all modes in the model for streamwise and azimuthal wavelengths, and this is shown in figure 2. It can be observed that the leading response mode contains more than 80 % of the total response over a large range of wavelengths, and for $\lambda_z > 1$ and $\lambda_\theta > 0.1$ what indicates that the operator is low rank. First, we investigate the effect of the choice of norm, with $\alpha = 0$ or $\alpha = 1$ and $\beta = 0$ or $\beta = 1$, on the relative gain of the first mode for various streamwise and azimuthal wavenumbers with a phase speed, $c_w = \overline{u}_z(y^+ = 15)$ for $St^+ = 0.1 - 1$ and $g_i = 0$ in figure 2. When $\alpha = 1, \beta = 0$, shown in figure 2 (left column), the gain plots become independent of St and Fr which is obvious since only the Navier-Stokes equations are considered. The gain plot then becomes identical to similar plots in for instance McKeon & Sharma (2010) or Luhar *et al.* (2014*b*). Similarly, when $\alpha = 0$, $\beta = 1$, shown in figure 2 (middle column) the gain plot is also constant when $\frac{1}{Fr} = 0$, which shows that equation 11 in this case is independent of Stokes number as well. It is important to note that in equation 11 only the concentration fluctuations are taken into consideration, so there are no interactions with the fluid velocity. Finally, by setting $\alpha = 1$, $\beta = 1$ (right column), the two previous gain plots combine. Here, it seems like the low rank behaviour is switched from the $\lambda_\theta = 2\pi$ ($k_\theta = 1$) to $\lambda_\theta = 2\pi/3$ ($k_\theta = 3$) for the largest streamwise modes ($\lambda_z > 200, k_z < 1$). It seems the main effect of increasing the Stokes number is to increase the low order nature of the smallest streamwise wavenumbers. This could indicate the existence of local clustering, observed in among others Marchioli *et al.* (2007). This could also help explain the existence of the long narrow clusters of particles observed near the wall, which are often much longer and narrower than velocity streaks, (Sardina *et al.* (2012); Brandt & Coletti (2022)).

Next, the effect of Fr is tested, by looking at the gain from equation 11 which is the simplified system in figure 3 at two wave speeds, $c_w = \overline{u}_z(y^+ = 15)$ figure 3 (top row), and $c_w = \overline{u}_z(y^+ = 150)$ figure 3 (bottom row). Figure 3a,d show the case of no gravity, figure 3b,e show the case of a downward flow and figure 3c,e show an upward flow. Here we observe that by increasing St/Fr, We increase the low-rank region for upward flow in the near wall region, and reduce it for the downward flow as seen in the top row. Similarly, we increase the low-rank region in further from the wall for a downward flow and reduce it for the upward flow as shown in bottom row. Similar observations for the mean and rms particle concentrations were also made in the Lagrangian simulations of Nilsen *et al.* (2013) and Capecelatro & Desjardins (2015).

The flow structures are now analysed using the resolvent framework as shown in figures 4 for the full system and 5 for the simplified equation modes. The most energetic scales for the various Stokes and Froude numbers under consideration for the different wall-normal heights still coincide somewhat with the passive scalar case, even though the inertial and gravitational effects changes which exact wavelengths causes the system to become low rank. However, to simplify the analysis, it is necessary to limit the analysis to only a few modes. We therefore analyse the mode $k_z = \pi/2$, $k_\theta = 4$ since it is low rank at the different wavespeeds, $c_w(y^+ = 15), c_w = \overline{u}_z(y^+ = 30), c_w = \overline{u}_z(y^+ = 120)$, as well as the special case of the locally clustered mode, which is shown at $k_z = 10\pi$, $k_\theta = 4$, $c_w = \overline{u}_z(y^+ = 150)$ which was shown to increase in gain with increasing St^+. We plot $\sigma_1|\phi_{1,c}|$ to show both the shape of the mode, but also its relative importance.

In figure 4, the most energetic mode for at the different wave speeds is plotted for no-gravity (top row), downward (middle row) and upward flow (bottow row). The main effect of increasing the Stokes number is shown in figure 4a-d and seems to be to amplify the locally clustered modes, further away from the wall. This is primarily done for smaller more narrow shapes. This is caused by particles moving to regions of lower turbulence intensity, which has also been observed in for instance Sardina *et al.* (2012). The effect of downward flows, shown in figure 4e-h, show that the concentration peak of the modes moves somewhat closer to the wall for the smaller modes. Furthermore, the concentration fluctuations seems to increase significantly in the bulk region of the flow. This is also observed in several Lagrangian simulations, of Nilsen *et al.* (2013) and Capecelatro & Desjardins (2015). In Nilsen *et al.* (2013), the increase in the bulk region was explained with downward gravity increasing the average particle velocity and therefore aligning the particles more with faster moving bulk flow structures, whereas the opposite is the case for upward flow. The effect of the upward flow, figure 4i-l, seems to move the peak somewhat away from the wall, but to increase them in the log region their amplitude when compared to the downward or no-gravity flow. This was also shown in Nilsen *et al.* (2013), where the concentration in the logarithmic region increased for upward flows. In both the upward and downward flow, we see that the gravitational effects seem to dominate the inertial effects, since figure 4h,l no longer show the effect of inertia. This would change if the Stokes number was increased, or the gravitational effect was reduced.

Finally, the flow is analysed using the simplified resolvent operator described in equation 11 in figure 5 for the same values as in 4. As in figure 5, $\sigma|\phi_{1,c}|$ is plotted in order to show both the shape of the mode, but also the relative magnitude. In figure 5 we can see that inertial effects no longer plays a role, since the no gravity case of figure 5a-d no longer changes with Stokes number. However, gravitational effects still seem to be visible. For a downward flow, figure 5e-h, it can still

be observed that the modes are mainly amplified closer to the centre, whereas, for the upward flow, figure 5i-l, the modes are amplified in the log layer of the wall.

Despite using only a few modes for this representation, the overall features of the flow concentration intensities are still captured, with an increase in the bulk region of the flow for the downward flow, and an increase in the near-wall region of the flow for the upward flow, and finally, a sharp increase for locally clustered modes when the Stokes number is increased. The gravitational effects can be found using the simplified system, which means that the mean concentration profile is not needed. The gravitational effect of particles can therefore be analysed for a wide range of Reynolds numbers, provided only the velocity profile is obtained first.

CONCLUSION AND FUTURE WORK

In this paper, we investigated the transport and wall transfer in a turbulent pipe flow at $Re = 5300$ (based on bulk velocity) using the equilibrium Eulerian model for particle velocity and adapted the model to the resolvent framework. The equilibrium Eulerian model was validated against other experiments and simulations and was found to correctly capture the trends observed in no gravity, upward and downward vertical turbulent pipe flows. The resolvent methodology presented has allowed us to analyse which modes become amplified depending on their Stokes and Froude number. It was found that the resolvent model was able to capture the characteristics of inertial particles in wall-bounded effects. The model predicted the occurrence of smaller regions with a high concentration of particles, that the bulk region of the flow gets amplified for downward flows and that the near-wall region gets amplified for upward flows. The trends solely related to the direction of gravity could be observed using a simplified resolvent model, that did not require concentration profiles. This means that key insight can be provided into these types of flows, in a few seconds, using a standard laptop. Finally, the model also showed how gravity affects particle distribution. It was shown that modes in the log region become amplified in upward flow and that downward flow amplifies modes in the centre, but also moves some modes closer to the wall.

Future work will explore the potential of the methodology for gaining insight into more complex settings that may include chemical reactions and different flow configurations. The current configuration of the resolvent model was closed using mean velocity and concentration profiles. The model could become more sophisticated by modelling the forcing term of the resolvent operator which would make it possible to obtain accurate flow statistics such as rms values. Other future work includes using the resolvent operator for flow control to modify deposition of inertial particles, as was done for a velocity only analysis of a turbulent pipe flow by Luhar *et al.* (2014*a*).

ACKNOWLEDGEMENTS

We would like to thank the UK Turbulence Consortium and the UK Materials and Molecular Modelling Hub for computational time at ARCHER and THOMAS via EPSRC Grant No. EP/R029326/1 and (EP/P020194/1), and the Leverhulme Trust (RPG-2018-101) for financial support.

REFERENCES

Ahmed, M. A., Bae, H. J., Thompson, A. F. & McKeon, B. J. 2021 Resolvent analysis of stratification effects on wall-bounded shear flows. *Physical Review Fluids* **6** (8), 1–25.

Brandt, Luca & Coletti, Filippo 2022 Particle-Laden Turbulence: Progress and Perspectives. *Annual Review of Fluid Mechanics* **54** (1), 159–189.

Capecelatro, Jesse & Desjardins, Olivier 2015 Mass Loading Effects on Turbulence Modulation by Particle Clustering in Dilute and Moderately Dilute Channel Flows. *Journal of Fluids Engineering, Transactions of the ASME* **137** (11).

Dawson, Scott T.M., McKeon, Beverley J. & Saxton-Fox, Theresa 2018 Modeling passive scalar dynamics in wall-bounded turbulence using resolvent analysis. *2018 AIAA Fluid Dynamics Conference* p. 4042.

Ferry, J. & Balachandar, S. 2001 A fast Eulerian method for disperse two-phase flow. *International Journal of Multiphase Flow* **27** (7), 1199–1226.

Ferry, Jim, Rani, Sarma L. & Balachandar, S. 2003 A locally implicit improvement of the equilibrium Eulerian method. *International Journal of Multiphase Flow* **29** (6), 869–891.

Luhar, M., Sharma, A. S. & McKeon, B. J. 2014*a* On the structure and origin of pressure fluctuations in wall turbulence: Predictions based on the resolvent analysis. *Journal of Fluid Mechanics* **751**, 38–70.

Luhar, M., Sharma, A. S. & McKeon, B. J. 2014*b* Opposition control within the resolvent analysis framework. *Journal of Fluid Mechanics* **749**, 597–626.

Marchioli, Cristian, Picciotto, Maurizio & Soldati, Alfredo 2007 Influence of gravity and lift on particle velocity statistics and transfer rates in turbulent vertical channel flow. *International Journal of Multiphase Flow* **33** (3), 227–251.

McKeon, B. J. 2017 The engine behind (wall) turbulence: Perspectives on scale interactions. *Journal of Fluid Mechanics* **817**, 1–86.

McKeon, B. J. & Sharma, A. S. 2010 A critical-layer framework for turbulent pipe flow. *Journal of Fluid Mechanics* **658**, 336–382.

Nilsen, Christopher, Andersson, Helge I. & Zhao, Lihao 2013 A Voronoï analysis of preferential concentration in a vertical channel flow. *Physics of Fluids* **25** (11).

Oliveira, J. L.G., Van Der Geld, C. W.M. & Kuerten, J. G.M. 2017 Concentration and velocity statistics of inertial particles in upward and downward pipe flow. *Journal of Fluid Mechanics* **822**, 640–663.

Sardina, G., Schlatter, P., Brandt, L., Picano, F. & Casciola, C. M. 2012 Wall accumulation and spatial localization in particle-laden wall flows. *Journal of Fluid Mechanics* **699** (May 2014), 50–78.

Sharma, A. S. & McKeon, B. J. 2013 On coherent structure in wall turbulence. *Journal of Fluid Mechanics* **728**, 196–238.

Veenman, MPB 2004 Statistical analysis of turbulent pipe flow: A numerical approach. PhD thesis, Eindhoven University of Technology.

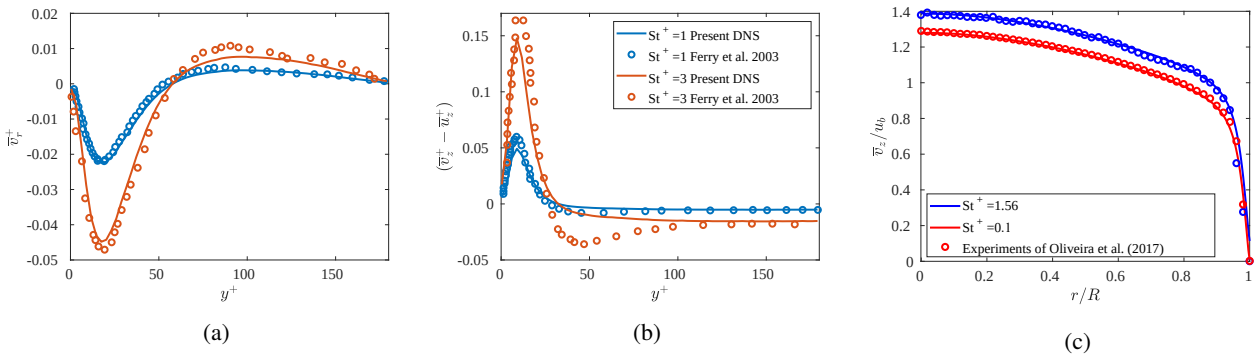

Figure 1: Wall-normal particle velocity (a) and difference between streamwise average particle velocity and fluid velocity (b) of a channel flow simulation with $Re_\tau = 180$ compared to the Lagrangian simulation from Ferry *et al.* (2003), where solid lines are the present simulations and (o) are the Lagrangian simulation, blue line color is $St^+ = 1$ and red line color is $St^+ = 3$. Velocity profiles for particles with $St^+ = 0.1$ and $St^+ = 1.56$ for a downward flow with $Re_B = 10300$, compared with an experiment by Oliveira *et al.* (2017) (c).

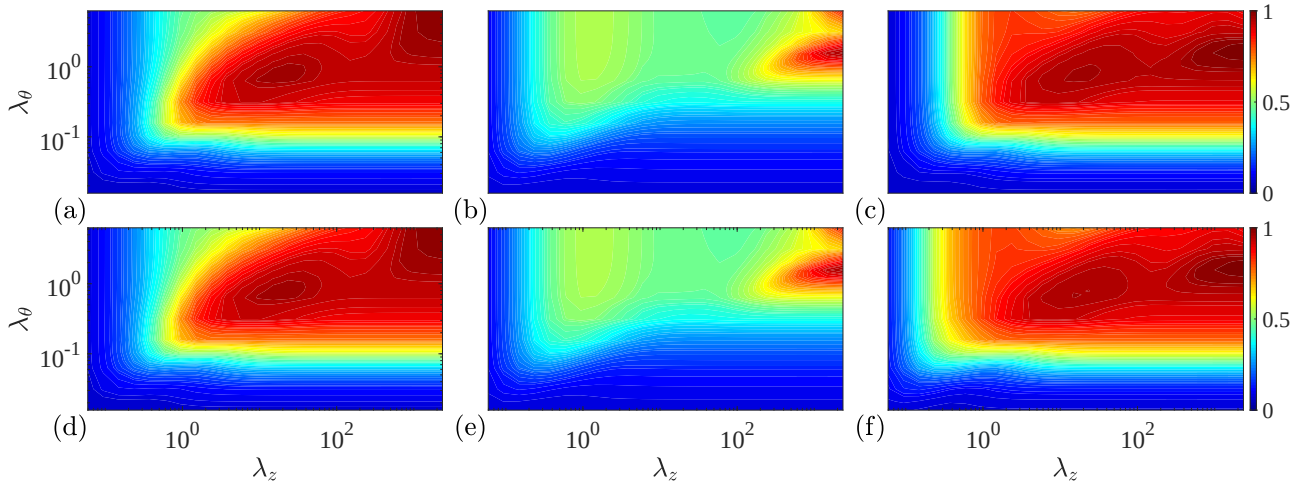

Figure 2: Contour plots of the energy contained in the leading response mode relative to all modes, $\sigma_1^2/\sum_{n=1,N_r}\sigma_n^2$ for $c_w = \overline{u}(y^+ = 15)$, where the resolvent is found using a norm with kinetic energy, $\alpha = 1, \beta = 0$, (left column) the simplified resolvent operator from equation 11, $\alpha = 0, \beta = 1$, (middle column), and kinetic energy and particles, $\alpha = 1, \beta = 1$, (right column), where (top row) is for $St^+ = 0.1$ and (bottom row) is for $St^+ = 1.0$ and $\frac{1}{Fr} = 0$.

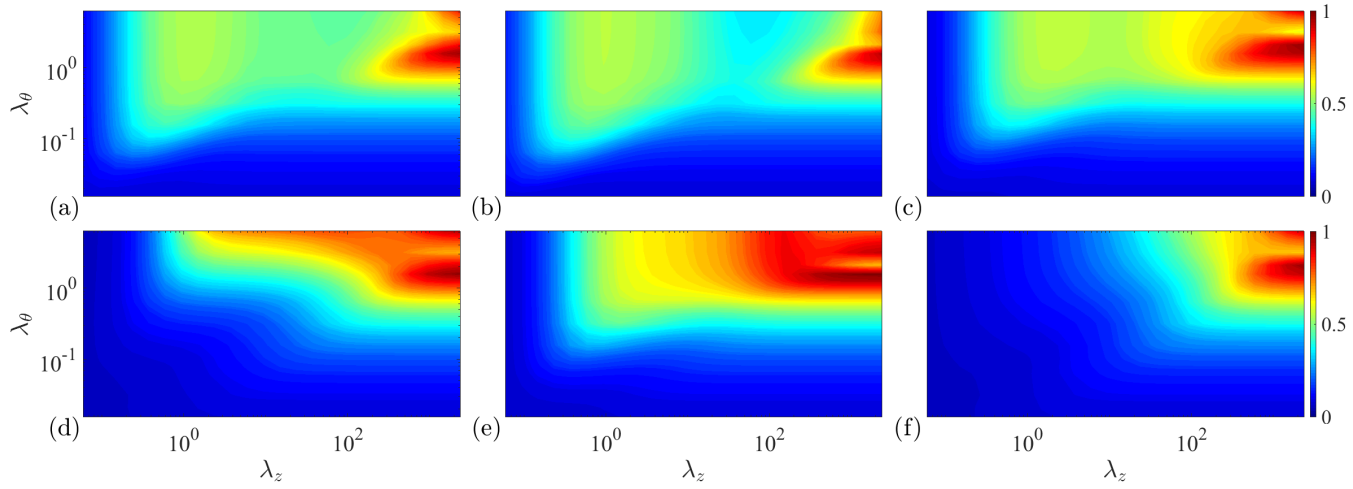

Figure 3: Contour plots of the energy contained in the leading response mode relative to all modes, $\sigma_1^2/\sum_{n=1,N_r}\sigma_n^2$ for $c_w = \overline{u}_z(y^+ = 15)$ (top row) and $c_w = \overline{u}_z(y^+ = 150)$ (bottom row), for the simplified equation 11, i.e $\alpha = 0, \beta = 1$. (left column) $1/Fr = 0$ (i.e. zero gravity), $St^+ = 1$, (middle column) $Fr = 0.4$, (right column) $Fr = -0.4$.

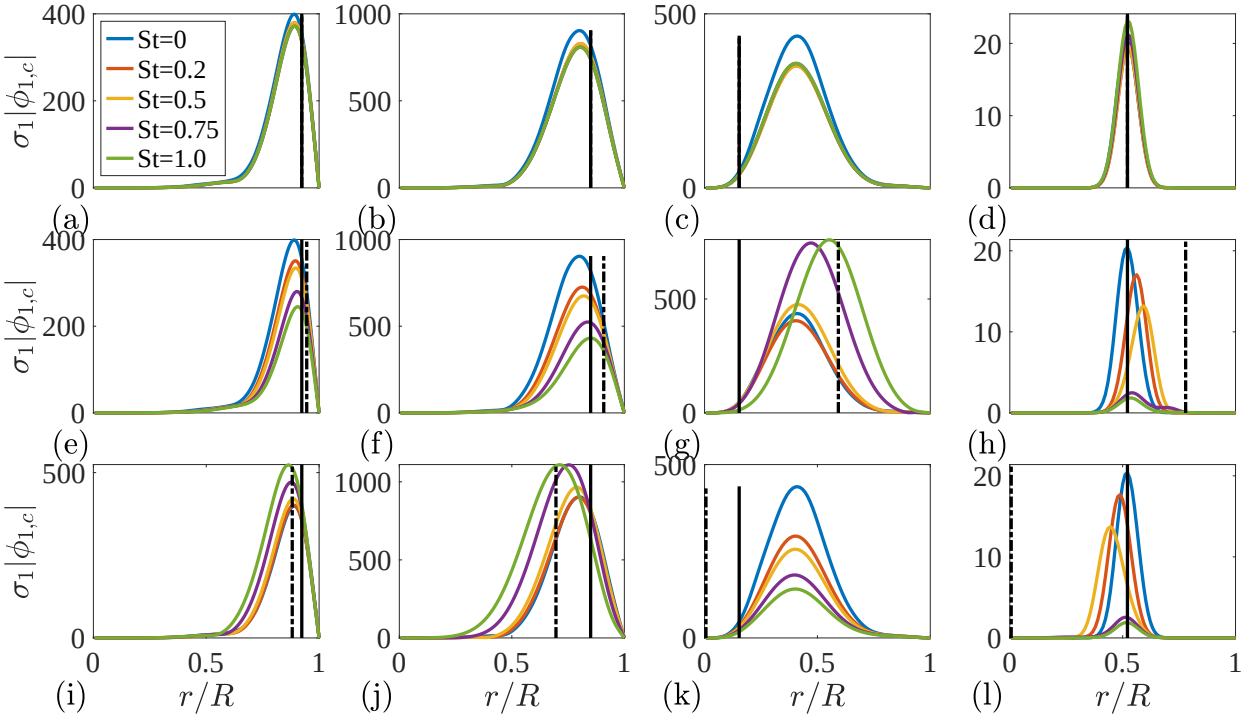

Figure 4: Mode shapes for concentration fluctuations for no gravity (a-d), downward (e-h) and upward flow (i-l), where (a,e,i) is for $c_w = \overline{u}(y^+ = 15)$, (b,f,j) $c_w = \overline{u}(y^+ = 30)$, (c,g,k) $c_w = \overline{u}(y^+ = 150)$ and (d,h,l) is for local clustering. The black vertical line indicate the location of the critical layer of the velocity field, and the dashed-dotted vertical line is the location of the critical layer for the concentration profile.

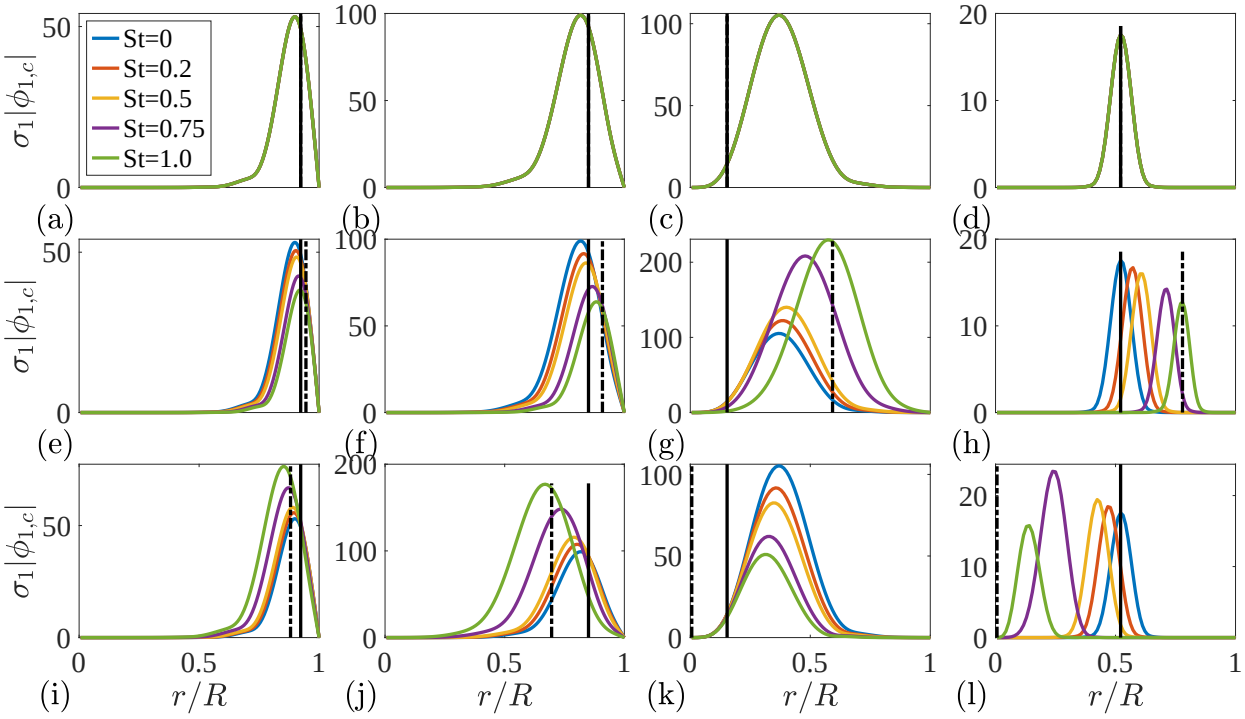

Figure 5: Mode shapes for concentration fluctuations of the simplified resolvent mode described in equation 11 for no gravity (a-d), downward (e-h) and upward flow (i-l), where (a,e,i) is for $c_w = \overline{u}(y^+ = 15)$, (b,f,j) $c_w = \overline{u}(y^+ = 30)$, (c,g,k) $c_w = \overline{u}(y^+ = 150)$ and (d,h,l) is for local clustering. The black vertical line indicate the location of the critical layer of the velocity field, and the dashed-dotted vertical line is the location of the critical layer for the concentration profile.